HIFAN 1668

Exact solution of the envelope equations for a matched quadrupole-focused beam in the low space-charge limit

O. A. Anderson, LBNL, Berkeley, CA 94720, USA
L. L. LoDestro, LLNL, Livermore, CA 94551, USA

Accelerator Fusion Research Division
Ernest Orlando Lawrence Berkeley National Laboratory
University of California
Berkeley, California 94720

September 2008

This work was supported by the Director, Office of Science, Office of Fusion Energy Sciences, of the U.S. Department of Energy under Contract No. DE-AC02-05CH11231.

Exact solution of the envelope equations for a matched quadrupole-focused beam in the low space-charge limit

O. A. Anderson, LBNL, Berkeley, CA 94720, USA
L. L. LoDestro, LLNL, Livermore, CA 94551, USA

The Kapchinskij-Vladimirskij equations are widely used to study the evolution of the beam envelopes in a periodic system of quadrupole focusing cells. In this paper, we analyze the case of a matched beam. Our model is analogous to that used by Courant and Snyder [E.D. Courant and H.S. Snyder, Ann. Phys. **3**, 1 (1958)] in obtaining a first-order approximate solution for a synchrotron. Here, we treat a linear machine and obtain an exact solution. The model uses a full occupancy, piecewise-constant focusing function and neglects space charge. There are solutions in an infinite number of bands as the focus strength is increased. We show that all these bands are stable. Our explicit results for the phase advance σ and the envelope $a(z)$ are exact for all phase advances except multiples of 180°, where the behavior is singular. We find that the peak envelope size is minimized at $\sigma = 90°$. Actual operation in the higher bands would require very large, very accurate field strengths and would produce significantly larger envelope excursions.

I. INTRODUCTION

The Kapchinskij-Vladimirskij (KV) equations describe the evolution of the beam envelopes in a periodic system of quadrupole focusing cells and are widely used to help predict the performance of such systems. When the focusing fields are moderately strong, numerical solutions are easily obtained. Problems can arise with very strong fields [1], especially when the phase advances are larger than 180°. Analytic solutions are often useful in the latter case and can provide helpful insight at any focus strength. Thus, there have been numerous analytic papers describing approximate solutions with varying degrees of accuracy.

In this paper, we present an exact solution for a matched beam, i.e., a beam whose envelope is periodic with the same period as the focusing lattice. We treat a problem examined by Courant and Snyder in their classic paper [2], except that we assume a linear rather than circular machine. They discussed the case in which the focus and defocus sections each had uniform focusing strength with no intervening gaps. They called this the CLS configuration [3]. Their model neglected space-charge, as we do in the present paper. Although space charge is no longer negligible in typical modern devices, the exact solution for this case does provide insight into the general behavior of alternating-gradient systems and can provide a starting point for analysis of other focusing models and the case of finite space charge.

Courant and Snyder used the CLS model for a synchrotron and obtained approximate solutions for the envelope and phase advance. Here, we show that the analogous model for a linear machine is exactly solvable and explore the consequences. (Lund and Bukh [4] have given an exact analysis for the opposite case: thin lenses with maximum space-charge intensity.)

In this paper, we refer to our analogous model (piecewise-constant focus, negligible space charge, linear beam axis) as the CSL model [5].

For the CSL model: (1) We find that solutions exist in an infinite number of bands coinciding with the bands of stability. (2) We obtain a well-defined expression for the phase advance σ as a function of focusing strength that applies to all bands. All values of σ are theoretically possible except exact multiples of 180°. (3) For fixed emittance, the peak beam radius is minimized when $\sigma = 90°$ and increases rapidly past that point. The higher bands give larger beam excursions in spite of greatly increased focusing fields [4], [6]. Although the minimum radius is reduced (cf. Ref. [7]), the average radius and the peak radius are increased. It is the peak radius that is significant for transport systems of fixed aperture. For such systems, in the emittance-dominated regime at least, there seems to be no advantage in increasing the focusing strength beyond the value that gives $\sigma = 90°$ — except possibly for special applications, such as those discussed in Sec. X.

II. FOCUSING MODEL

We assume a quadrupole-symmetric focusing function $K(z)$ that is piecewise constant with values $\pm k$ and periodic over a lattice with period $2L$. This model is described for the xz-plane by Eqs. (1) and Fig. 1:

$$K(z) = +k, \qquad 0 < z < L; \tag{1a}$$

$$K(z) = -k, \qquad L < z < 2L. \tag{1b}$$

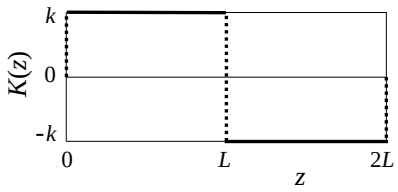

FIG. 1: CSL focusing model for the xz-plane. The yz-plane fields are the same but shifted by the distance L.

In a lattice with quadrupole symmetry, the xz-plane and yz-plane envelopes for a matched beam are identical except for a shift of length L [8], [9]. Thus, it is only necessary to analyze the dynamics in one of the planes; we choose the xz-plane here.

III. SINGLE-PARTICLE STABILITY

In the low space-charge limit, the vertical position $x(z)$ of a particle is determined by

$$x''(z) + K(z)x(z) = 0. \tag{2}$$

The stability of the single-particle orbit is easily found from the period-transfer matrix M [2], [10] and is given by $|\mathrm{Tr}(M)| < 2$. With $K(z)$ defined by Eq. (1), this yields

$$\left| \cos \sqrt{k}L \right| < \operatorname{sech} \sqrt{k}L. \tag{3}$$

Figure 2 shows that there are multiple bands of real solutions over increasingly narrow ranges of $\sqrt{k}L$.

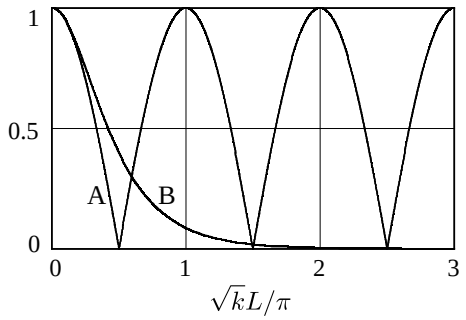

FIG. 2: A = $|\cos \sqrt{k}L|$; B = $\operatorname{sech} \sqrt{k}L$. Stable solutions exist in the regions where curve A lies below curve B.

IV. DERIVATION OF THE EXACT SOLUTION OF THE ENVELOPE EQUATIONS

In the CSL model, which neglects space charge, the xz-plane envelope $a(z)$ of a beam with emittance $\in$ obeys [10]:

$$a(z)'' + K(z)a - \frac{\in^2}{a^3} = 0 \tag{4}$$

with $K(z)$ from Eqs. (1). The boundary conditions are periodic for a matched beam.

Multiplying Eq. (4) by $2a'$ and integrating, one obtains

$$a'^2 + K(z)a^2 + \frac{\in^2}{a^2} = C\,. \tag{5}$$

Then, multiplying Eq. (5) by a^2 yields

$$dz = \frac{da^2}{2\sqrt{-K(z)a^4 + Ca^2 - \in^2}}\,. \tag{6}$$

Any standard table of integrals shows that the solution for $a^2(z)$ will involve trigonometric or hyperbolic functions, depending on the sign of K. We will find the appropriate constants by using trial solutions.

We define separate functions for the focus ($K = +k$) and defocus ($K = -k$) sections:

$$a(z) = \begin{cases} a_+(z) & \text{for } 0 < z < L \\ a_-(z) & \text{for } L < z < 2L \end{cases} \tag{7}$$

and choose trial solutions that satisfy the symmetry of $K(z)$:

$$\frac{\sqrt{k}}{\in} {a_+}^2(z) = \varphi + F\cos\lambda(z - L/2), \tag{8a}$$

$$\frac{\sqrt{k}}{\in} {a_-}^2(z) = \gamma + G\cosh\lambda(z - 3L/2), \tag{8b}$$

where $\lambda, \varphi, F, \gamma$, and G are constants. They will be determined by substituting Eqs. (8) into Eq. (4) and invoking continuity of values and derivatives of a_+ and a_- at the junctions.

For the focus section, we differentiate Eq. (8a) twice and find after some algebra that

$${a_+}'' = -\frac{\lambda^2}{4} a_+(z) \left(1 + \frac{\in^2}{k} \frac{F^2 - \varphi^2}{{a_+}^4}\right). \tag{9}$$

Comparison with Eq. (4) gives

$$\lambda = 2\sqrt{k}, \tag{10}$$

the first of the five unknown constants, and

$$\varphi^2 = F^2 + 1. \tag{11}$$

For the defocus section, Eq. (10) still applies and we find similarly

$$\gamma^2 = G^2 - 1. \tag{12}$$

A. Introduction of the focus-strength parameter θ

The focus-strength parameter, used throughout this paper, is defined by

$$\theta \equiv \sqrt{k}L, \tag{13}$$

and our trial solutions become

$$\frac{\sqrt{k}}{\in} {a_+}^2(z) = \varphi + F\cos\theta(2z/L - 1), \tag{14}$$

$$\frac{\sqrt{k}}{\in} {a_-}^2(z) = \gamma + G\cosh\theta(2z/L - 3), \tag{15}$$

The first derivatives are

$$\frac{\sqrt{k}}{\in} {a_+}^2(z)' = -(2\theta/L)F\sin\theta(2z/L - 1), \tag{16}$$

$$\frac{\sqrt{k}}{\in} {a_-}^2(z)' = +(2\theta/L)G\sinh\theta(2z/L - 3). \tag{17}$$

We introduce the following quantities that depend only on the focus-strength parameter:

$$sn(\theta) \equiv \sin\theta, \qquad cs(\theta) \equiv \cos\theta,$$
$$sh(\theta) \equiv \sinh\theta, \qquad ch(\theta) \equiv \cosh\theta, \tag{18}$$

$$\rho \equiv sn/sh. \tag{19}$$

For simplicity, we drop the arguments of sn, cs, sh, and ch henceforth.

B. Continuity conditions

The four remaining unknown constants, φ, F, γ, and G, are found by invoking continuity of a and a' at $z = L$, the boundary between focus and defocus sections. The symmetries built into our trial solutions guarantee periodicity of $a(z)$ with period $2L$.

Using Eqs. (16) and (17), we equate derivatives at $z = L$:

$$G = \rho F. \tag{20}$$

We equate $a_+{}^2(L)$ and $a_-{}^2(L)$ using Eqs. (14) and (15):

$$\gamma - \varphi = (cs - \rho\, ch)F. \tag{21}$$

For our four unknowns we now have four equations: (11), (12), (20) and (21). The first three yield

$$\varphi^2 + \gamma^2 = (1 + \rho^2)F^2. \tag{22}$$

From Eq. (21),

$$\gamma^2 + \varphi^2 - 2\gamma\varphi = (cs - \rho\, ch)^2 F^2. \tag{23}$$

Combining Eqs. (22) and (23) yields

$$\gamma\, \varphi = F^2 \rho\; ch\, cs. \tag{24}$$

We square this and use Eqs. (11) and (12). After a little more algebra, we find

$$\rho^2(1 - cs^2 ch^2)F^4 - (1 - \rho^2)F^2 - 1 = 0. \tag{25}$$

The real solutions are $F = \pm(\rho^2 ch^2 - 1)^{-1/2}$ with F negative for $\pi < (\theta - 2\pi n) < 2\pi$. We write

$$F = \frac{\mathrm{P}}{\sqrt{\rho^2 ch^2 - 1}} = \frac{\mathrm{P}\, sh}{\sqrt{1 - cs^2 ch^2}}, \tag{26}$$

where

$$\mathrm{P}(\theta) \equiv \mathrm{sign}(sn). \tag{27}$$

From Eq. (11), $\varphi = \mathrm{P}\; sn\; ch(1 - cs^2 ch^2)^{-1/2}$. The P function is required here since, according to Eq. (8a), φ is necessarily positive. The P function in Eq. (26) then ensures that $a_-{}^2$ maintains a positive value for any θ [see Eqs. (15) and (20)].

C. Exact solution

Finally, then, Eqs. (14) and (15) yield the exact solution

$$a_+{}^2(z) = \in L\, \frac{sn\, ch + sh \cos[\theta(2z/L - 1)]}{\mathrm{P}\, \theta\sqrt{1 - cs^2 ch^2}}, \tag{28a}$$

$$a_-{}^2(z) = \in L\, \frac{sh\, cs + sn \cosh[\theta(2z/L - 3)]}{\mathrm{P}\, \theta\sqrt{1 - cs^2 ch^2}}, \tag{28b}$$

where the second equation utilizes Eqs. (20) and (21).

Figure 3 plots $a(z)/\sqrt{\in L}$ for various focusing strengths θ within the stable pass bands discussed below. Equations (28) have real solutions (pass bands) when their denominators are real. The existence criterion is

$$cs^2 ch^2 < 1. \tag{29}$$

This agrees with the stability criterion, Eq. (3), showing that a solution is stable if it exists.

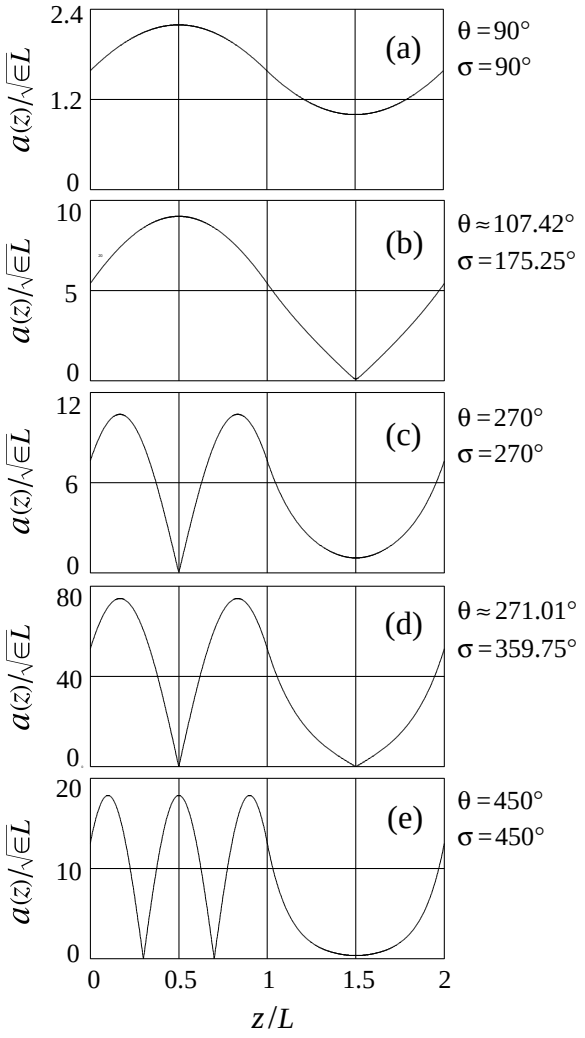

FIG. 3: Plots of Eqs. (28) for various focusing strengths θ with fixed emittance $\in$: (a) θ=0.5π, midpoint of the first stable band; (b) θ=0.5968π, near band 1 edge; (c) θ=1.5π, the midpoint of band 2; (d) θ=1.50561868π, near band 2 edge; (e) θ=2.5π, band 3 midpoint. Peak radius is smallest where θ and σ are 90° — see Figs. 5 and 6. (The phase advance σ is discussed in Sec. V.) The minimum of the envelope $a(z)$ can be very small but it is always finite. In the even bands, $a(z)$ and $b(z)$ have minima at the same z values. Therefore, in case (d) there are huge reductions in beam area at $z = L/2$ and $3L/2$. (See Figs. 8 and 9.)

V. PHASE ADVANCE IN THE STABLE BANDS

The matched solution of Eq. (4), Eqs. (28), has stable bands which surround the points where $cs = 0$. We call these the midpoints θ_n for the focus-strength parameter:

$$\theta_n \equiv (n - \tfrac{1}{2})\pi \qquad n = 1, 2, 3 \cdots \tag{30}$$

where n is the pass-band number.

From Ref. [2], the full-period phase advance $\sigma(\theta)$ for the CSL case is (assuming $|cs\,ch| < 1$),

$$\cos\sigma = \tfrac{1}{2}\,\mathrm{Tr}\,M = \cos\theta\cosh\theta. \tag{31}$$

(Note that $\cos\sigma = 0$ when $\cos\theta = 0$, so that $\sigma_n = \theta_n$.)

In the higher pass bands, the sign of $\sigma(\theta)$, obtained from Eq. (31), is ill-defined. To avoid ambiguity, we introduce the deviations $\Delta\theta$ and $\Delta\sigma$, defined by

$$\theta = \theta_n + \Delta\theta; \qquad \sigma = \theta_n + \Delta\sigma, \tag{32}$$

where $-\frac{\pi}{2} < \Delta\sigma < \frac{\pi}{2}$ and where $\Delta\theta$ has a smaller range (extremely small for $n > 1$). Substitution of Eqs. (32) into Eq. (31) gives

$$\sin\Delta\sigma = \sin\Delta\theta\ \cosh\theta \tag{33}$$

with $|\sin\Delta\theta\,\cosh\theta| < 1$. Then

$$\sigma(\theta) = \theta_n + \sin^{-1}(\sin\Delta\theta\ \cosh\theta). \tag{34}$$

Here, $\sin^{-1}$ is restricted to the principal value, removing the ambiguity. Figure 4 displays $\sigma(\theta)$ for the first two bands.

From Eq. (34) and Fig. 4 we see that, for any band n, σ has maximum and minimum values

$$\sigma_{\max} = n\pi, \qquad \sigma_{\min} = (n-1)\pi. \tag{35}$$

In all pass bands, σ ranges over 180°, so that arbitrary σ is possible except for the singular points $\sigma = n\pi$. The required precision of k becomes extreme near these points.

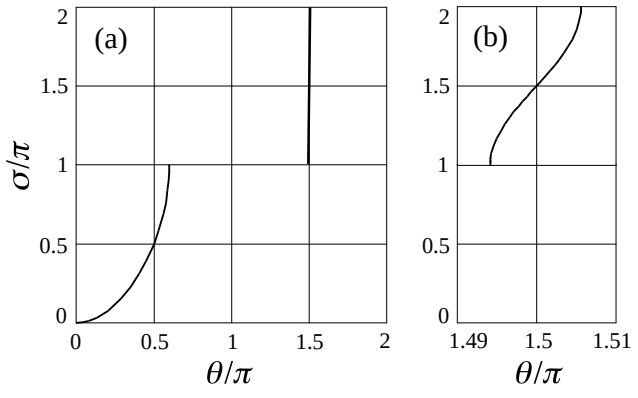

FIG. 4: (a) Phase advance [Eq. (34)] for the first two stable bands. (b) The second band again with the θ axis magnified.

VI. MAXIMUM ENVELOPE EXCURSION

The peak radius $a_{\max}$ is found from Eq. (28a) by setting the cosine term (containing z) equal to P, yielding:

$$\frac{a^2_{\max}(\theta)}{\in L} = \frac{\mathrm{P}\,sn\,ch + sh}{\theta\sqrt{1 - cs^2 ch^2}}. \tag{36}$$

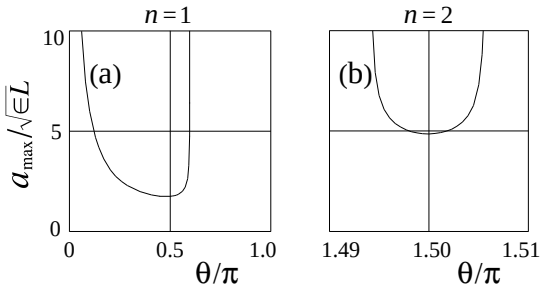

FIG. 5: (a) Values of $a_{\max}/\sqrt{\in L}$ [Eq. (36)] for the first stable band. (b) The second band with the θ axis magnified. The smallest possible envelope excursions occur for $\theta = 90°$.

Figure 5 illustrates Eq. (36), showing $a_{\max}/\sqrt{\in L}$ as a function of θ for the first two stable bands. In Fig. 5(a), the peak radius $a_{\max}$ decreases with increasing field strength up to the point where θ and σ reach 90°. Further increase of θ causes a rapid increase in the peak radius, which diverges as σ approaches 180°. In the narrow second band, the peak radius has a minimum value where θ and σ are very close to 270°.

The peak radius at the center of any band (essentially the minimum peak radius) is found by setting $\theta = \theta_n$:

$$a_{+\max}^2(\theta_n) = \in L\frac{e^{\theta_n}}{\theta_n}, \tag{37}$$

where θ_n is given by Eq. (30). From this, one finds that the minimum peak radius in the second band is about 2.78 times larger than in the first band and that it increases almost exponentially for larger n.

With the CSL model, then, for given $\in$ and L the smallest peak radius occurs when the phase advance is 90°.

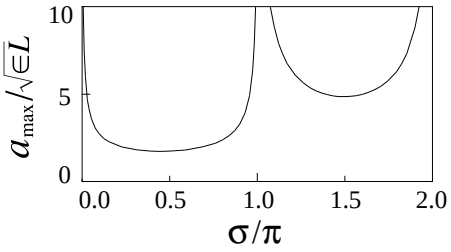

FIG. 6: Values of $a_{\max}/\sqrt{\in L}$ [Eq. (36)] for the first two stable bands as a function of phase advance σ [Eq. (34)]. Minimum beam size occurs at $\sigma = 90°$.

Figure 6 shows $a_{\max}$ for the first two bands in terms of the phase advance σ rather than the field-strength parameter used for Fig. 5. As mentioned at the end of Sec. V, all the pass bands have width 180°. The stop bands [4], in the absence of space charge, shrink to points at 180°, 360°, etc.

VII. PHASE ADVANCE AS A FUNCTION OF z FOR PASS-BAND MIDPOINTS

At the midpoints θ_n, the cosine factor containing z in Eq. (28) becomes

$$\cos\theta\left(\frac{2z}{L}-1\right)=\sin\left(\theta_n\frac{2z}{L}\right) \tag{38}$$

and the denominators become $\mathrm{P}\,\theta$. Thus, a^2 at the midpoint of any band n is

$$a_{n+}{}^2(n;z)=\in L\frac{ch_n+sh_n\,\mathrm{P}\sin(\theta_n 2z/L)}{\theta_n} \tag{39a}$$

$$a_{n-}{}^2(n;z)=\frac{\in L}{\theta_n}\cosh[\theta_n(2z/L-3)]. \tag{39b}$$

The reciprocals of Eqs. (39) are easily integrated (using appropriate branch selection), yielding the exact phase advance $\sigma(\theta;z)$ along the z-axis:

$$\sigma(\theta;z)=\in\int_0^z\frac{dz'}{a^2} \tag{40}$$

where the θ-dependence enters through a. The integral is done in sections. We illustrate for band 2, where $\theta_2=\frac{3\pi}{2}$.

$$\sigma(\theta_2;z)\;=\;\begin{cases}\tan^{-1}(e^{\theta_2}\tan x)-\tan^{-1}e^{\theta_2}+\begin{cases}0, & 0<z<\frac{1}{6}L\\ \pi, & \frac{1}{6}L<z<\frac{5}{6}L\\ 2\pi, & \frac{5}{6}L<z<L\end{cases}\\ \tan^{-1}(e^{y})-\tan^{-1}e^{\theta_2}+\frac{3}{2}\pi, & L<z<2L,\end{cases}$$

where

$$\begin{aligned}x\;&\equiv\;\tfrac{1}{2}\theta_2(\tfrac{2z}{L}-1)\\ y\;&\equiv\;\theta_2(\tfrac{2z}{L}-3)\end{aligned} \tag{41}$$

and where the principal values of $\tan^{-1}$ are used. The phase advance over a full period $(0,2L)$ is $3\pi/2$, which agrees with Eq. (34) for θ_2. The above result is plotted in Fig. 7.

VIII. SECOND-BAND BEAM COMPRESSION

Figure 3 shows that, in the second band, the beam radius is small in both the x and y directions for $z/L=0.5$ and for $z/L=1.5$ so that the beam area is highly compressed at these points. (Recall that $b(z)=a(z+L)$ for our matched beam.) The beam area is plotted on linear and log scales for the center (Fig. 8) and the edge (Fig. 9) of the second band. The KV equation predicts that the compression ratio is more than 200 in the former case and more than 10^7 in the latter. However, various effects not taken into account by the CSL model will limit the beam compression. These and other practical matters are discussed in Sec. X.

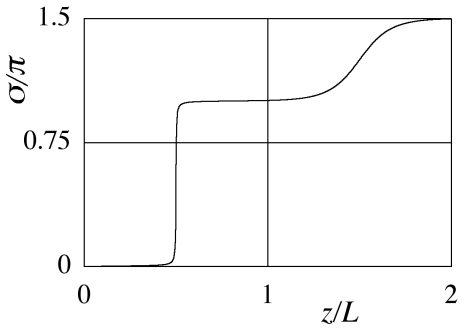

FIG. 7: Phase σ as a function of z for the center of the second stable band, from Eq. (41). Note the phase jump at $z=L/2$.

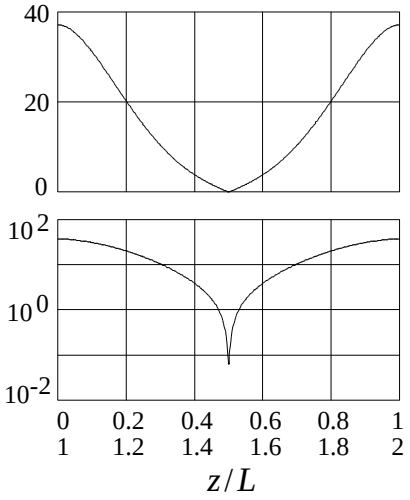

FIG. 8: Normalized beam area $\pi a(z)a(z+L)/\in L$ as a function of z for the center of the second band. Focus-strength parameter $\theta=1.5\pi;\sigma=270°$. (Cf. Fig. 3c.)

IX. BEAM MATCHING EQUATION

We now return to Eq. (28a) and restrict z to a constant value, z_0, regarding the right-hand side as a function of θ, $\in$, and L. For $z_0=0$, this yields $a_0=f(\theta,\in,L)$. That is, we have obtained a matching condition relating the initial beam amplitude and the parameters θ, $\in$, and L. In the limit $\theta\to 0$, we find $a_0^2\to 2\sqrt{3}\in L/\theta^2$, the usual smooth-approximation matching condition [11].

From another viewpoint, we observe that Eq. (4), together with periodic K and the requirement that the beam be matched to the lattice, is a homogeneous system with periodic boundary conditions. This leads us

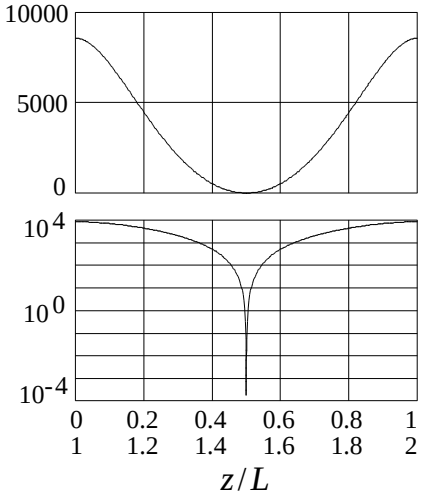

FIG. 9: Normalized beam area $\pi a(z)a(z+L)/\in L$ as a function of z near the edge of the second band. Focus-strength parameter $\theta = 1.50561868\pi; \sigma = 359.75°$. (Cf. Fig. 3d.)

to interpret the solution of the envelope equations for matched beams as an eigenvalue problem. The matching condition is then understood as the (nonlinear) equation for the eigenvalues. As typically occurs for nonlinear problems, the eigenfunction normalization, of which a_0 is a measure, enters the eigenvalue equation.

Specifically, we observe that Eq. (36) is a transcendental equation for θ, the eigenvalue. (The measure is $a_{\max}$ instead of a_0—the difference is unimportant.) Some modes of its spectrum are indicated graphically in Fig. 5. One sees that the ordinate value $a_{\max}/\sqrt{\in L} = 5$ intersects the plot twice in each of the first two bands; it has no intersections in higher bands. There is a total of four modes in this example.

X. DISCUSSION OF THE SECOND BAND

For charge-dominated beams, some authors, e.g. [7], have recommended operating in higher bands to transport larger beam current. Lund has pointed out that the envelope excursions will then increase [4]. Emittance-dominated beams also exhibit this excursion increase, as shown by Eq. (37). For a given aperture, the particle flux is reduced in the higher bands. Nevertheless, there may be some uses for the second band, assuming such operation to be feasible in practice.

In the emittance-dominated case, the second band has a special feature: The beam radii in both planes can be small at the same point, as noted in Fig. 3. These localized regions of high compression discussed in Sec. VIII suggest some possible applications. For example, the hot, extremely dense spots, if achievable, may themselves be of interest. The small beam area could lend itself to schemes for differential pumping of the beam line using diaphragms.

The design of a machine for second-band operation would face formidable difficulties. Compared with the focusing field for $\sigma = 90°$, the field for 270° is nine times stronger. The narrowness in θ of the second band would require accurate field regulation—extremely accurate if operating near the band edge as in Fig. 9. It would be difficult to launch a beam in the second band. Launching at $z = 0$, for example, would require steeply converging and diverging envelope angles in the two symmetry planes. All these would be technical challenges.

Effects have been neglected in this paper that would reduce the beam compression. Large beam excursions will produce focusing aberrations, not treatable by the KV equations with their paraxial approximation. As mentioned above, significant space-charge fields will widen the focus. (However, this may be mitigated since emittance pressure eventually dominates as the beam is compressed.) All these effects remain to be studied.

A final remark applies to any band: The full KV equations, which include space charge terms, require the KV distribution function [10] for the beam in order to produce the linear transverse self-field required for a periodic solution. The beam density is uniform with a sharp cutoff at the boundary. On the other hand, periodic solutions can be obtained with the CSL model using distributions that give realistic density profiles.

Acknowledgments

We thank Ed Lee for helpful suggestions and Steve Lund for his many comments and his help with an early draft. Supported in part by the U.S. Department of Energy under Contract DE-AC03-76SF00098.

[1] S. M. Lund, S. H. Chilton, and E. P. Lee, Phys. Rev. ST-AB **9**(064201) (2006).
[2] E. D. Courant and H. S. Snyder, Ann. of Phys. **3**, 1 (1958).
[3] In Ref. [2], CLS refers to an earlier paper by Courant, Livingston, and Snyder. See Ref. [2], pp. 2 and 15.
[4] S. M. Lund and B. Bukh, Phys. Rev. ST-AB **7**, 024801 (2004).
[5] CSL stands for "Courant-Snyder, Linear axis".
[6] E. P. Lee and R. J. Briggs, Tech. Rep. LBNL-40774, UC 419, Lawrence Berkeley National Laboratory (1997).
[7] R. Pakter and F. B. Rizzato, Phys. Rev. E **65**, 056503 (2002).
[8] E. P. Lee, Phys. Plasmas **9**, 4301 (2002).
[9] O. A. Anderson, Phys. Rev. ST-AB **10**(3), 034202 (2007).
[10] H. Wiedemann, *Particle Accelerator Physics* (Springer-Verlag, New York, 1993).
[11] M. Reiser, Particle Accelerators **8**, 167 (1978).